

Gravity waves over Antarctica and the Southern Ocean: consistent momentum fluxes in mesoscale simulations and stratospheric balloon observations

Riwal Plougonven,^{a*} Albert Hertzog^b and Lionel Guez^a

^aLaboratoire de Météorologie Dynamique, École Normale Supérieure, IPSL, Paris, France

^bLaboratoire de Météorologie Dynamique, École Polytechnique, IPSL, Palaiseau, France

*Correspondence to: R. Plougonven, LMD, École Normale Supérieure, IPSL, 24 rue Lhomond, Paris 75005, France.
E-mail: plougon@lmd.ens.fr

Stratospheric balloons from the Vorcore campaign have provided a unique description of the gravity-wave field in the lower stratosphere above Antarctica and the Southern Ocean, during the austral spring of 2005. Mesoscale simulations are carried out to analyze further the gravity-wave field. First, the realism of the simulated waves is assessed by comparison to the observations. A satisfactory overall agreement is found, but different behaviour is noted for orographic waves (overestimation in the simulations relative to the observations) and non-orographic waves (underestimation). Second, the gravity-wave field is analyzed in more detail than was possible from observations alone. It is necessary to distinguish and quantify orographic and non-orographic waves separately. Orographic waves are larger and more intermittent, yet affect only a limited geographical region. Hence, although orographic sources stand out as ‘hot spots’ for gravity waves, their contribution to momentum fluxes entering the stratosphere is comparable to or smaller than the contribution of non-orographic sources. A diagnostic for intermittency, the Gini coefficient, is proposed. It clearly marks the distinction between orographic and non-orographic sources (intermittencies of ~ 0.8 and ~ 0.5 respectively). Sensitivity to resolution is quite small regarding the spatial structure of the gravity-wave field, but is significant for the amplitudes. The momentum flux values increase by ~ 2 when the horizontal resolution is doubled, and possible biases of both simulations and observations are discussed. Nonetheless, the good agreement between observations and simulations and the complementary information on the biases of each dataset promises that in the future these different estimates of gravity-wave momentum fluxes may converge. Copyright © 2012 Royal Meteorological Society

Key Words: Vorcore; orographic waves

Received 20 December 2011; Revised 26 March 2012; Accepted 30 March 2012; Published online in Wiley Online Library 7 June 2012

Citation: Plougonven R, Hertzog A, Guez L. 2013. Gravity waves over Antarctica and the Southern Ocean: consistent momentum fluxes in mesoscale simulations and stratospheric balloon observations. *Q. J. R. Meteorol. Soc.* **139**: 101–118. DOI:10.1002/qj.1965

1. Introduction

Internal gravity waves (GWs) are ubiquitous in the atmosphere and play crucial roles in its dynamics, in

particular by transferring momentum upward from the troposphere to the middle atmosphere (Fritts and Alexander, 2003). Their intrinsic frequencies are higher than the inertial period, and consequently they generally occur on rather

short spatial scales mostly ranging from a few kilometres to several hundreds of kilometres, i.e. scales on which the Rossby number $U/(fL)$ can be of order unity or larger. Only recently has it become possible to begin constructing a global description of these waves from observations (e.g. Ern *et al.*, 2004) and from high-resolution modelling (e.g. Sato *et al.*, 1999). One specific purpose for describing the wave field is to provide constraints for climate modellers who need to include parametrizations to represent the effects of these waves (Kim *et al.*, 2003).

The key effect due to GWs that is represented by parametrizations is the vertical transport of momentum from lower layers of the atmosphere to the middle atmosphere, where the waves eventually break. As climate models extending to the middle atmosphere become more common (e.g. Lott *et al.*, 2005; Eyring *et al.*, 2007; Morgenstern *et al.*, 2010), it becomes more and more necessary to improve deficiencies in these parametrizations. As a result of the vertical propagation and selective filtering, the deposition of momentum which occurs in the mesosphere closes the mesospheric jets (Andrews *et al.*, 1987). GWs also contribute to the stratospheric circulation, and the uncertainties in the parametrizations contribute to the uncertainties in the models (Austin *et al.*, 2003; Morgenstern *et al.*, 2010).

Approaches needed to improve current parametrizations of GWs include better observational constraints and high-resolution simulations (Alexander *et al.*, 2010). Super-pressure balloons are well suited for observing internal GWs; because the balloons drift as quasi-Lagrangian tracers, they provide direct access to the intrinsic frequencies of the phenomena they sample. The Vorcore campaign (Hertzog *et al.*, 2007) consisted of 27 super-pressure balloons launched during the austral spring of 2005, from 5 September to 28 October. The last balloon fell on 1 February 2006. Each balloon drifted for about two months, providing measurements of position, pressure and temperature every 15 min. Using a wavelet analysis (Boccaro *et al.*, 2008), the GWs were analyzed in these *in situ* observations, providing an unprecedented climatology of GW momentum fluxes over the whole of Antarctica and the surrounding oceans up to 50°S (Hertzog *et al.*, 2008).

Our goal is to achieve a better quantification and understanding of the GW field, and in particular of the tropospheric GW sources. For that purpose, mesoscale simulations have been carried out in a large domain ($10\,000 \times 10\,000$ km, up to 5 hPa) and for a long period (2 months) during the Vorcore campaign. High spatial resolutions have been used ($\Delta x = 20$ km and 10 km) to ensure a good description of most of the GW field. The choice of the domain and period was guided by two specific opportunities: the large dataset available from the balloon observations of Vorcore makes it possible to assess in detail the realism of the simulation. The domain covered includes a major *hot spot* of GW activity (Ern *et al.*, 2004), but also vast oceanic regions, where non-orographic waves will dominate.

Hence, the present investigation lies between individual case-studies (e.g. Wu and Zhang, 2004; Doyle *et al.*, 2005; Alexander and Teitelbaum, 2007; Limpasuvan *et al.*, 2007) and high-resolution general circulation model (GCM) simulations (e.g. Jones *et al.*, 1997; Hamilton *et al.*, 1999; Sato *et al.*, 1999; Kawatani *et al.*, 2008). Case-studies compare observations and numerical simulations, but only

in a limited domain and for one, or a few, case(s). High-resolution GCM studies provide global insight into the wave field, but only allow statistical comparison with observations, i.e. with no specific observational counterpart for the simulated wave events*.

The two main objectives of the present study are (1) to compare the simulated and the observed GW fields, and (2) to use the simulations to quantify variations in time and space of the GW field. A central issue will be the distinction between orographic (OGW) and non-orographic (NGW) waves. This distinction reflects on essential physical differences (stationary versus non-stationary waves), and a considerable gap in our understanding and in our ability to parametrize (e.g. Kim *et al.*, 2003). Sources for non-orographic waves cover a wide range of processes (jets, fronts, shear, convection—these not being mutually exclusive, on the contrary). In global investigations of GWs, localized maxima due to orographic waves are often found to dominate (Ern *et al.*, 2004; Alexander *et al.*, 2008), and focus much of the attention. However, NGW need also to be carefully analyzed (perhaps even more so), first because they have different physical properties (non-zero phase speeds) and effects, and second because of the pressing need for improving their parametrizations.

The article is organized as follows: section 2 describes the numerical set-up. The comparison with the balloon observations is carried out in section 3. The simulations are then used to describe the variations in time and space of the GW field at the height of the balloons (section 4), and their variations with height (section 5). The sensitivity of the results is investigated in section 6. Section 7 provides the conclusions and a discussion of the results.

2. Numerical set-up

The mesoscale simulations were carried out with the Weather Research and Forecast Model (WRF; Skamarock *et al.*, 2008). The precise configuration was determined based on a preliminary sensitivity study (Plougonven *et al.*, 2010). The period was chosen to include significant coverage by the balloons, in particular of oceanic regions, and the chosen domain was large enough to include significant oceanic regions. Figure 1 shows the trajectories of the balloons during the period considered and the density of observations; a large fraction of the trajectories occur over the Southern Ocean, making it possible to investigate non-orographic sources of GWs.

The domain is $10\,000$ km \times $10\,000$ km (Figure 1), with a horizontal resolution of $dx \sim 20$ km, and uses a Lambert conformal projection. In the vertical direction, 120 levels are used up to 5 hPa, i.e. about 36 km, with levels roughly equidistant (every 300 m). A timestep of 60 s was used.

A succession of runs each lasting three days was made, with an overlap of one day between successive runs. The initial condition and the boundary conditions for each simulation were prepared from the analyses of the European Centre for

*High-resolution simulations that do not include GW parametrizations yet describe a realistic middle atmosphere provide valuable insights on the GW field, but possibly need cautious interpretation: only part of the spectrum of atmospheric GWs is resolved (the sources and dissipation could both be better resolved), yet the effects in the middle atmosphere seem adequately described. The model is doing the right thing, but not necessarily with the right waves.

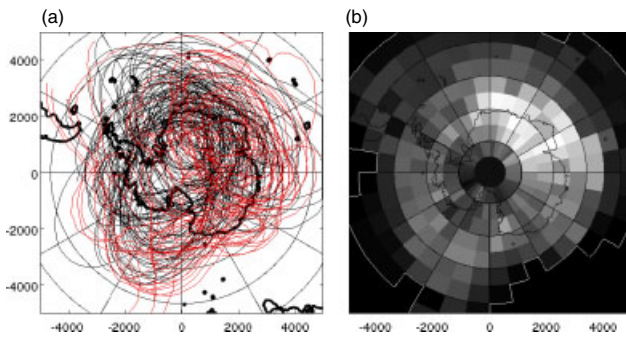


Figure 1. (a) Domain for the simulations and trajectories of the Vorcore balloons from 0000 UTC on 21 October to 0000 UTC on 18 December 2005. Trajectories are black for the first 29 days, then have a lighter hue. (b) number of 'observations' available for each box (5° latitude \times 10° longitude). The maximum (white) is 3628 balloon measurements, which would be equivalent to nearly 38 days of continuous measurements if only one balloon were present at a time. This figure is available in colour online at wileyonlinelibrary.com/journal/qj

Medium-range Weather Forecast (ECMWF). An alternative could have been to try and obtain a single, continuous run, with the advantage that simulated time series along the balloon trajectories could have been produced (whereas our succession of overlapping runs rules this out). However, nudging or assimilation would have been necessary to maintain the flow close to the analyses. It was chosen not to follow this route in order to avoid the possibility of spurious GW generation, and to let the model freely produce mesoscale features.

The choice of 24 h for the spin-up time (or equivalently for the overlap between two successive simulations) resulted from our preliminary experiments (Plougonven *et al.*, 2010), and agrees with common practice. The length of each simulation (3 days) appeared as a reasonable compromise to keep the flow close to the analyses, given the predictability of the large-scale flow at such latitudes. The parametrization of the microphysics uses the WRF single-moment 5-class scheme, and the Noah Land Surface Model is used for the land surface, as recent modifications have been added for processes over ice and snow (Wang *et al.*, 2009). As an illustration, Figure 2 shows a snapshot of the tropospheric flow and of the stratospheric GW field over one quarter of the domain, for 1200 UTC on 24 November 2005. There are several features to note: in the troposphere, fronts and extratropical cyclones found around Antarctica are well described within the domain. The vertical velocity field in the lower stratosphere mainly consists of small-scale features that are typical of GWs. Strikingly, there is a clear similarity between the structure of the GW field and the structure of the tropospheric flow. Note also that strong GW activity often coincides with strong values of the local wind.

3. Comparison with observations

Our purpose is to compare the GW field in the simulations and in the balloon observations. The two key questions are whether the spatial structure and the amplitudes agree. The chosen quantity for comparison is momentum fluxes, given its importance for global modelling (Alexander *et al.*, 2010) and its use in previous studies of balloon observations (Hertzog *et al.*, 2008).

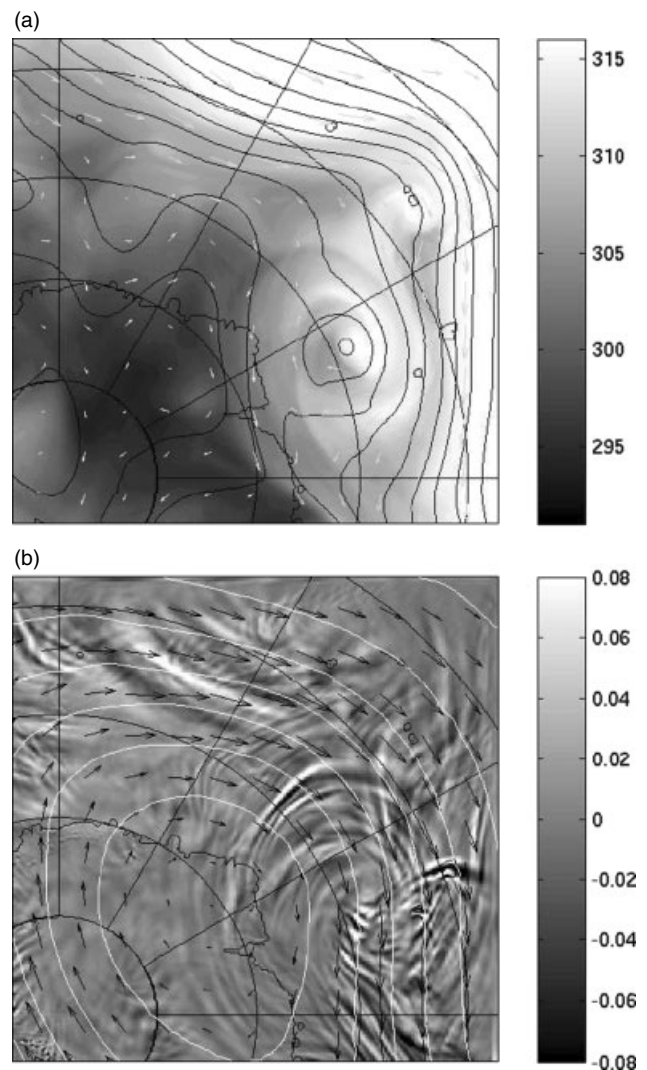


Figure 2. (a) Potential temperature (shading), pressure (contours, every 5 hPa) and wind in the upper troposphere ($z = 8$ km), for 1200 UTC on 24 November 2005. (b) Vertical velocity (shading), pressure (white contours, every 2 hPa) and wind in the lower stratosphere ($z = 17$ km). For vertical velocity, the range is limited to $|w| < 0.08$ m s^{-1} , although maximum values reach ~ 0.4 m s^{-1} . Latitude circles are drawn every 10° , and meridians every 30° , with the Greenwich meridian pointing upward to the top of the figure.

3.1. Calculation of momentum fluxes

In the long-duration balloon dataset, the observed time series of pressure, zonal and meridional velocities are used to obtain the vertical flux of GW total, zonal and meridional momentum. Namely, a wavelet analysis is performed in order to separate the GW disturbances from those induced by the longer planetary waves, as well as to isolate GW packets in the time series (Boccaro *et al.*, 2008; Hertzog *et al.*, 2008). Due to the sampling used during Vorcore, the analysis is restricted to GWs with intrinsic periods longer than 1 h. In order to provide, on the one hand, a dataset comparable with the output of the numerical simulations and, on the other hand, statistically significant values, the balloon momentum fluxes are averaged for 6 h into 10° longitude by 5° latitude geographical boxes.

In the numerical simulations, the horizontal wind (x and y components along the WRF grid) and vertical wind are interpolated at different heights. The balloons fly at heights

between 17 and 19 km, depending on their diameter (8.5 and 10 m balloons were used during the campaign), and so the simulations are analyzed at $z = 18$ km for comparison with the balloons. Fluxes actually show little sensitivity to height in the altitude range of the balloons (cf. section 5). For each output time (every 6 h), the large-scale part of the fields is identified using a moving filter with a Hamming window of width 1000 km. The horizontal velocities are only then converted to zonal and meridional velocities. The zonal and meridional momentum fluxes are then calculated as $u' w'$ and $v' w'$ at each grid point. Unless stated otherwise, the obtained fluxes are not smoothed spatially; the time average over the whole period and the spatial averaging into geographical boxes similar to the Vorcore dataset suffice. Last, we restrict our analysis to regions sufficiently far from the domain boundaries (i.e. poleward of 50°S).

3.2. Overall comparison

The momentum fluxes calculated from the simulations at $z = 18$ km and from the balloons, averaged over the period 0000 UTC on 21 October to 0000 UTC on 18 December 2005, are displayed in Figures 3 (zonal) and 4 (meridional). Each figure shows four panels: (a) the simulated momentum fluxes averaged over the whole period, (b) the same but spatially averaged to boxes as for the Vorcore observations, (c) the same but with the same sampling in time as in the balloon observations and (d) the fluxes estimated from the Vorcore balloons. These values are somewhat difficult to plot because of the large disparity between the largest values (e.g. -24.2 mPa for zonal momentum fluxes in 'boxes' using all simulated times, -47.8 mPa when using Vorcore temporal sampling, and -10.9 mPa for Vorcore data) and the vast majority of values (more than 90% are smaller, in absolute value, than 1 mPa). We are dealing with very large extrema concentrated in a small area (the Antarctic Peninsula). In consequence, the colour range for Figures 3 and 4 had to be chosen carefully; a choice based on extreme values reveals only the extreme values above the Antarctic Peninsula, dominating all other regions and hence hiding any structure present over the rest of the domain.

Examination of the time-averaged zonal momentum fluxes (Figure 3) reveals two striking features:

1. The orders of magnitude of the momentum fluxes in the simulations and in the observations are comparable. In fact, the spatial average of the zonal momentum fluxes over the whole domain (cf. the last line of Table 2) are nearly identical for the simulations with Vorcore sampling (-0.92 mPa) and for the observations (-0.90 mPa). This coincidence of course reveals some luck (compensating errors), but it is nonetheless remarkably satisfactory regarding the realism of the simulations.
2. The Antarctic Peninsula produces, by far, the largest local values for average momentum fluxes. This is found consistently in the observations and in the simulations, though momentum fluxes are larger there in the simulations than in the observations, as discussed further below.

A third feature is the satisfactory agreement in spatial variations over the oceans. The structures here are not as conspicuous, but regions of enhanced fluxes between -55°

Table 1. The seven different regions used for the analysis. The fraction of the total area represented by each region is shown as a percentage.

Region	Description	Area (10^6 km ²)	%
1	Antarctic Peninsula	3.7	5.1
2	Antarctic Coastline	13.6	18.9
3	Islands	4.5	6.3
4	Tip of the Andes	2.1	2.9
5	Southern Ocean	39.9	55.4
6	Drake Passage	1.7	2.4
7	Antarctic Plateau	6.6	9.1

and -50° S around 105° E and around 105° W for example are found to coincide.

3.3. Regional comparison

In order to analyze more precisely the different components of the GW field, we identify and compare different regions. Decomposing the domain into orographic and oceanic regions is a convenient proxy to decompose the wave field into orographic and non-orographic components. Different regions will correspond to different GW sources: OGWs will have a dominant contribution over regions like the Antarctic Peninsula, whereas jets, fronts and possibly convection (i.e. NGWs) will be the sources responsible for waves over the Southern Ocean[†]. We need to distinguish between these different regions, otherwise we are comparing apples and oranges: the model (and the observations) may have certain biases for OGWs and different biases for NGWs. These are different phenomena, with different scales and characteristics. In GCMs, they are represented by separate parametrizations, and this is a further motivation to try and quantify separately both components of the GW field.

The domain is decomposed into seven regions, described in Table 1 and shown in Figure 5. The two main regions to be compared and contrasted will be the Antarctic Peninsula (region 1), where the largest fluxes are found, and the oceans (region 5), away from topographic features and islands, where only NGWs are expected. Similarly, Hertzog *et al.* (2008) had decomposed the region covered by the balloon observations into two regions, based on the intensity of the gradient of orography. Our decomposition differs in three ways: first, regions around orographic sources have simpler shapes (so that they can be used by others for comparison) and are broader, especially downstream in order to allow for wakes (cf. discussion in Plougonven *et al.*, 2010). Second, we isolate regions that will be useful for specific discussions (e.g. islands and Drake Passage). Third, we distinguish between NGW regions which are close to the storm tracks (oceans) and far from it (Plateau).

The average momentum fluxes for each region, and the contribution to the domain average expressed as a percentage are reported in Table 2[‡]. Results are shown for the simulations over all times, the simulations with Vorcore-like temporal sampling, and the balloon observations.

[†]We here use the term Southern Ocean loosely: it is defined by the International Hydrographic Organization as the ocean poleward of 60° S. However, our analysis extends to 50° S, and hence into the southernmost parts of the Atlantic, Indian and Pacific Oceans.

[‡]This is obtained as the regional average times the area of the region, divided by the total area of the seven regions, so that the domain average is the sum of the seven contributions.

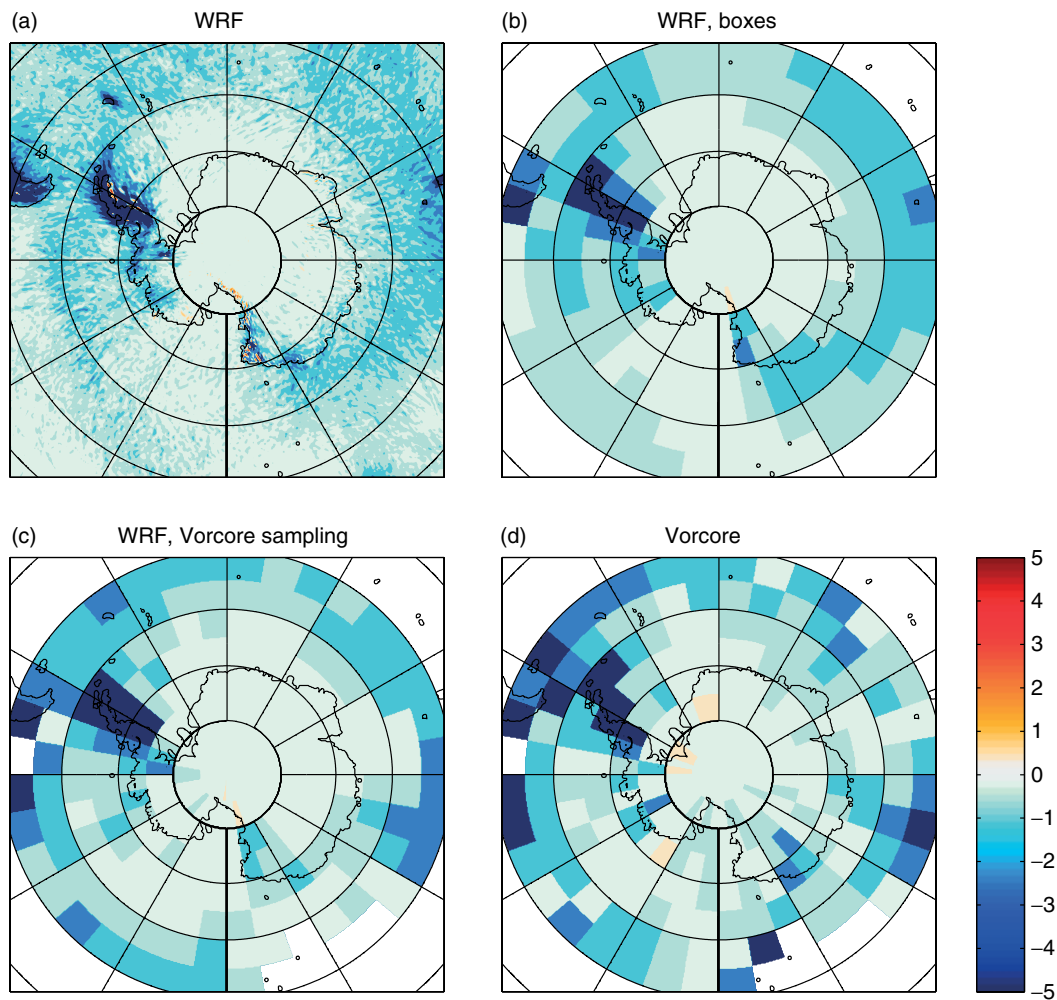


Figure 3. Time-averaged zonal momentum fluxes (a, b, c) from the simulations at $z = 17$ km and (d) from balloon observations between 16 and 19 km. The simulated fluxes are shown (a) with full resolution, (b) averaged on the same grid as the Vorcore data, and (c) sampled at the same times as Vorcore balloons. The colour range has been restricted to $[-5, 5]$ mPa, since otherwise only the extreme values near the Antarctic Peninsula would be visible.

Table 2. Mean zonal momentum fluxes and contribution to the integrated fluxes for each of the seven different regions, for simulations using all times, for simulations with Vorcore temporal sampling, and for the observations.

Region	Simulation (all times)		Simulation (Vorcore times)		Vorcore observations	
	Flux (mPa)	Contribution (%)	Flux (mPa)	Contribution (%)	Flux (mPa)	Contribution (%)
Antarctic Peninsula	-3.4	27.3	-6.5	38.2	-2.6	15.8
Antarctic Coastline	-0.35	10.3	-0.26	5.5	-0.31	6.8
Islands	-0.60	6.0	-0.93	5.1	-1.10	6.2
Tip of the Andes	-1.90	8.6	-2.30	7.5	-3.80	12.8
Southern Ocean	-0.50	44.1	-0.67	40.3	-0.83	50.5
Drake Passage	-0.70	2.6	-1.00	2.8	-2.50	6.8
Antarctic Plateau	-0.06	0.9	-0.06	0.6	-0.11	1.2
All regions	-0.63	100	-0.92	100	-0.90	100

As stated above, the overall average compares well between observations and simulations with Vorcore-like temporal sampling. The domain average over all simulated times is 30% less intense. This is mostly due to the uneven sampling of the whole period by the balloons. The last balloon was launched on 28 October, and hence the number of balloons decreases from that date. In consequence, the number of $10^\circ \times 5^\circ$ boxes containing observations generally decreases with time, introducing a bias towards the beginning of the period. As the absolute value of momentum fluxes decreases

over the period, this bias results in a bias towards larger absolute values.

The Antarctic Peninsula is the region over which the values differ most between observations and simulations. The average estimated from the observations is -2.6 mPa, its simulated counterpart being -6.5 mPa, i.e. 2.5 times larger. Two factors account for this. Most importantly, the time resolution of the balloon observations is only one measurement every 15 min, making waves with high intrinsic frequencies difficult to observe. For example,

the orographic wave studied in Plougonven *et al.* (2008) was sampled by only five measurement points from a balloon, yielding an underestimation relative to simulations by a factor 3 to 5. Secondly, the orographic waves are very localized in space, making them very sensitive to an inadequate sampling. In other regions of orographic waves (coastline, islands, tip of the Andes), the simulations compare well with the observations, with a slight underestimation.

Over the oceans (region 5), the simulations show a good agreement with the observations, with an underestimation of about 20%. It is of interest to note that, in contrast to the Antarctic Peninsula, the fluxes over the oceans are not as sensitive to the sampling. This is due to the larger size of the region, but also to the weaker intermittency and to the smoother evolution with time over the whole period (section 4).

To convey the relative importance of the different regions, one should not focus only on the mean values found there, but integrate these over the area of the region considered in order to obtain contributions to the overall mean (Table 2). The average fluxes due to NGWs over the oceans are significantly smaller than those due to OGWs over the Peninsula. In the observations, they are smaller by a factor of 3, yet their contribution to the integral of the fluxes over the seven regions is three times larger than that of GWs above the Peninsula. In the simulations, the average fluxes over the oceans are smaller by a factor of 7 than average fluxes over the Peninsula, yet their contribution is comparable to that from the Peninsula (with Vorcore sampling), or greater by a factor of 1.5 (all simulated times).

Another outcome from these comparisons is the sensitivity of the averages to the sampling in time. Comparison of Figures 3(b,c) and 4(b,c) indicates, encouragingly, that the spatial patterns do not vary much due to the limited temporal sampling. However, the average values of the fluxes do change: only by a factor of 1.3 over the oceans, but by a factor of 2 over the Peninsula. This indicates that the Vorcore sampling does have a significant impact. This is not limited to specific boxes having only few observations, but is general. As alluded to above, it is likely due to the decreasing number of Vorcore observations after the end of October, combined with the overall decrease in amplitudes of the momentum fluxes during the spring (section 4).

Above we have focused on contrasting regions 1 (Antarctic Peninsula) and 5 (oceans), representative of OGWs and NGWs respectively. The comparison between regions also shed light on specific issues. Islands of the Southern Ocean have recently been emphasized as a potentially important source of GWs (Alexander *et al.*, 2009). Our simulations and observations provide an estimate of the relative importance of these islands as responsible for about 5% of the total integrated fluxes poleward of 50°S, corresponding to mean fluxes that are equal to the domain average, or slightly smaller. In other words, our simulations and observations do not suggest clear evidence of an enhanced role of the islands as sources of GWs. However this statement has to be mitigated: several of the more important islands lie just outside the 50°S parallel, the topography of these islands may be inadequately resolved in the simulations, the season chosen may not be the most favorable, the sampling by the balloons of such limited areas is only very sporadic, and the OGW field there is expected to be very

intermittent. Moreover, the satellite observations (AIRS) used by Alexander *et al.* (2009) captures wavelengths down to 40 km, which is shorter than the limitation of the present simulations and balloon observations, and comparable to the width of South Georgia Island (30 km). Hence, our results provide only a crude lower bound of the flux over the Southern Ocean islands.

The Antarctic Plateau, including the South Pole, exhibits very weak momentum fluxes (about one order of magnitude smaller than the domain average in both simulations and observations). In consequence, this region hardly contributes at all to the momentum fluxes over the domain (about 1% or less, although it represents 10% of the area of the domain). In addition, we can note that the simulated average with Vorcore-like sampling is about half of its observational counterpart, suggesting that the simulations underestimate waves in this region. It could be an underestimation of waves propagating from the nearby orography, similar to what was detected in Plougonven *et al.* (2010).

The region of Drake Passage, extending over 800 km between the tips of South America and the Antarctic Peninsula has been isolated because it is unclear whether it would exhibit mostly NGWs, or OGWs propagating laterally from the nearby 'hot spots' (e.g. Wu and Jiang, 2002). The simulations exhibit momentum flux values in this region which are rather larger than those found over the oceans, but only by a factor of 1.4. In contrast to this, the fluxes derived from observations are comparable with those found over the Peninsula and the Andes (cf. regions 1, 4 and 6 in Table 2), and three times larger than fluxes over the oceans. In other words, the model here fails to reproduce a part of the GW field, again reminiscent of Plougonven *et al.* (2010). This may result from lateral propagation of relatively large-scale orographic waves (Sato *et al.*, 2012), but it is unclear why this would not be captured in the present simulations for that part of the orographic wave spectrum that is well resolved. The discrepancy between the simulated and observed wakes from topography calls for further research.

3.4. Meridional momentum fluxes

The meridional momentum fluxes have also been compared and the agreement is not as good. The overall average for the observed fluxes is -0.40 mPa, whereas the it is -0.16 mPa over all simulated times[§]. Hence, there is consistently a poleward flux, but its amplitude differs by up to a factor of 4 between observations and simulations. This difference results from mainly two factors: first, the simulations generally underestimate by about 30% the meridional fluxes, whether equatorward or poleward (the overall average of $|v' w'|$ is 0.92 mPa from the observations, and 0.61 mPa from the simulations over all times); second, the sign of the mean meridional fluxes over the Peninsula differs from the sign over the Southern Ocean (equatorward over the Peninsula, poleward over the oceans; Figure 4). Again, these signs are consistent between observations and simulations: over the Peninsula (region 1) observed fluxes are 0.09 mPa and simulated ones are 0.26 mPa. Over the oceans (region 5), they

[§]When using Vorcore sampling, the discrepancy is yet larger, with an overall average of -0.10 mPa. In the discussion of meridional momentum fluxes, for brevity only averages over all times are used for the simulated fluxes.

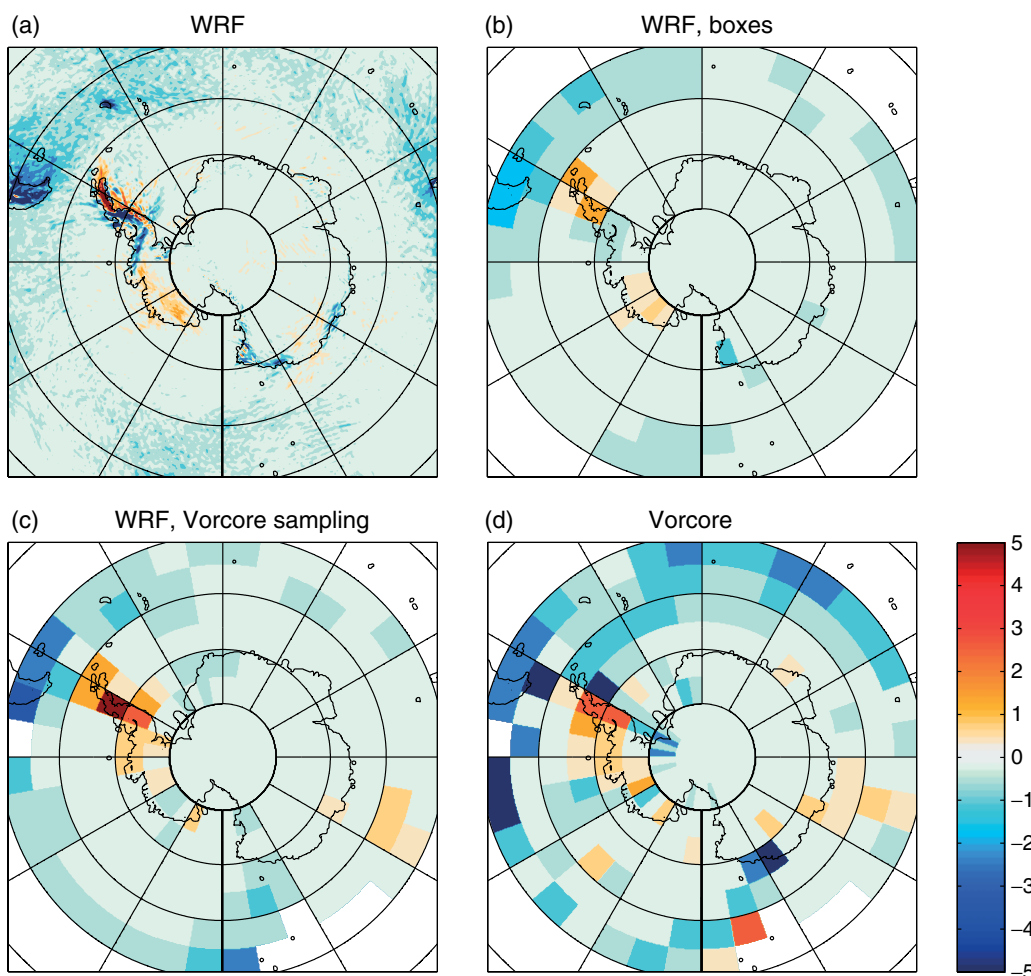


Figure 4. As Figure 3, but for meridional momentum fluxes.

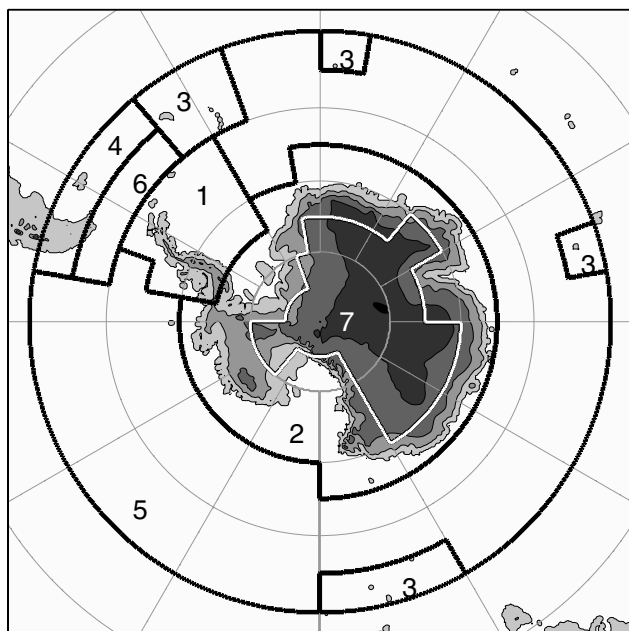


Figure 5. Decomposition of the domain into seven regions (Table 1) for the analysis of the gravity wave field.

are -0.48 mPa and -0.19 mPa respectively. Now, as was previously found for the zonal momentum fluxes, the simulations tend to overestimate the average of the absolute value

($|v'w'|$) over orography (over the Peninsula the observations yield 1.1 mPa and the simulations 1.4 mPa), and to underestimate the absolute value over the ocean (over region 5, the observations yield 0.72 mPa and the simulations 0.24 mPa). Now, the mean meridional momentum fluxes are a residual between equatorward (e.g. over the Peninsula) and poleward fluxes (e.g. over the oceans). The simulations overestimate OGW and underestimate NGW relative to the observations. Both effects result in positive biases for the meridional momentum fluxes, i.e. the biases add here, whereas they compensated each other for zonal momentum fluxes. Hence the agreement for the overall average appears rather poor relative to that found for zonal momentum fluxes.

3.5. Comparison of 6 h fluxes

Finally, one may push the comparison further and investigate to what extent momentum flux estimates at individual times (every 6 h) compare between the simulations and the observations. Figure 6 shows a scatterplot of the two estimates for zonal momentum fluxes, restricted to boxes for which at least 24 balloon observations were available (equivalent to one balloon flying per 6 h). Note that the simulated fluxes result from the analysis of instantaneous fields at time t , whereas the observed fluxes result from a time average of the fluxes estimated from the balloons in that box during $[t - 3 \text{ h}, t + 3 \text{ h}]$. Not surprisingly, there is significant scatter, and a number of outliers catch the eye.

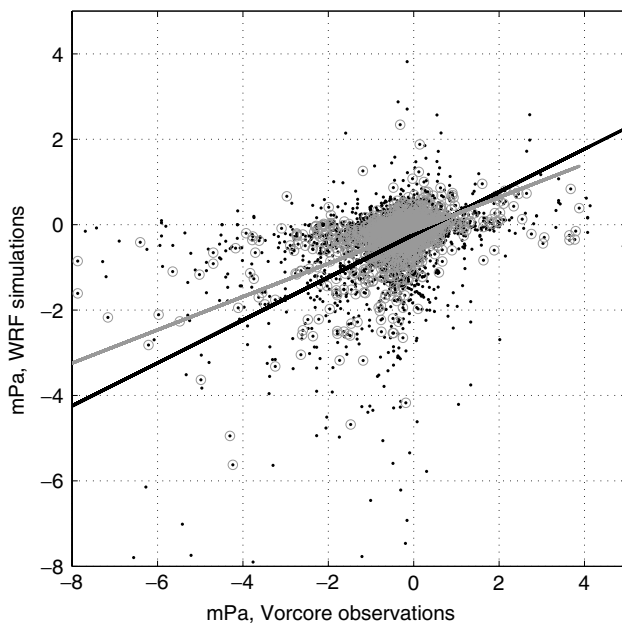


Figure 6. Scatterplot of zonal momentum fluxes estimated from the observations in boxes 10° longitude by 5° latitude and calculated from the simulations. Only boxes within which more than 6 hours of balloon flight were available were retained (black dots, 5269 values). A similar plot but with a more restrictive threshold of 12 hours of balloon flight is shown with grey open circles (1769 values). Black and grey lines show the linear regression, with slopes 0.50 and 0.39 respectively.

Indeed there is a scale issue on this figure (as in the maps): linear scales tend to emphasize the most intense events⁵. The correlation coefficient between the two sets of values is 0.28. Also shown is the set of points for which more than 48 balloon observations were available, and the correlation coefficient is then 0.49. Finally, a linear regression was carried out between observed and simulated fluxes. The lines, shown in Figure 6, have slopes of 0.50 and 0.39, for points with more than 24 and 48 balloon observations respectively. Moreover, they have negative values at the origin (-0.23 mPa and -0.14 mPa respectively). Such linear regressions will give more weight to events with significant fluxes, and results should hence be interpreted with caution. They indicate that the simulations generally underestimate the fluxes, particularly when they are large, by a factor of ~ 2 . On the other hand, there are a large number of small, negative values in the simulated fluxes that are not caught by the observations, which likely simply reflect the difficulty of capturing, even with wavelet analysis, weak GW events in the observations.

Given the uncertainties associated with the modelling (limitations of the model itself, of the resolution used, of the analysis used as initial and boundary conditions, and of the predictability of the background flow), and with the observations (limited geographical sampling and time resolution, limitations of the algorithm used to retrieve GWs and estimate momentum fluxes), this is quite satisfactory. Individual case-studies would be required to analyze further instances in which observations and simulations agree or fail to agree.

⁵An alternative analysis of the observed and simulated momentum fluxes consists of calculating and comparing their probability distribution functions. Such analysis has been carried out in detail in Hertzog *et al.* (2012), with an emphasis on the implications for intermittency.

4. Variability in time of the GW field

Time-averaged maps of momentum fluxes provide only part of the information needed to understand and parametrize the GW field. It is crucial to know how the momentum fluxes are distributed in time. A given mean zonal momentum flux can be due to a few very intense events, or numerous weak events. Now, in the absence of critical levels, a wave with larger amplitude is expected to become unstable and break at a lower altitude than a weaker wave (with the same wavenumber). In other words, the dissipation of numerous weak waves will occur higher than that of a few very intense events. The forcing due to these two distributions will completely differ. Hence knowledge of the mean should be complemented by information on the temporal distribution: time series (section 4.1) and diagnostics of the intermittency (section 4.2). A synthesis of the temporal variations of the wave field is provided by Hovmöller diagrams (section 4.3).

4.1. Time series

The time series of the average of zonal momentum flux over the whole domain is shown as the thin black curve in Figure 7. Not surprisingly, the values are always negative. Two features are striking. First, the absolute value decreases significantly in time, from values between -0.5 and -1 mPa in the first ten days to values between 0 and -0.3 mPa during the last ten days. This is consistent with the evolution of the background winds in the lower stratosphere, which change from strong westerlies to weak easterlies as the polar vortex breaks up toward the end of our simulations. Second, on top of this overall decrease in time, there are large episodic fluctuations, at least in the first half of the period. There is significant intermittency until approximately day 318, i.e. 14 November, with very intense periods lasting for a few days (days 302–304, 310–313, 316–317, i.e. 29–31 October, 6–9 November, 12–13 November), comprising very large fluctuations (several mPa), and quieter periods in between. After day 318, the evolution of the domain average zonal momentum flux is smoother, with much weaker fluctuations (e.g. the peak at day 335, 1 December).

It is useful to decompose this time series into contributions from the seven different regions described by Table 1 and Figure 1. As expected from Table 2, the contributions from the Antarctic Peninsula (region 1), which has the most intense local values for the fluxes, and from the Southern Ocean (region 5), which covers the largest fraction of the domain, dominate the signal.

However, the time series reveal how different the temporal variabilities of the fluxes in the two regions are: strikingly, the wild fluctuations seen in the domain average between days 300 and 318 are entirely due to the contribution from the Antarctic Peninsula. In other words, there are episodes of very intense orographic waves over the Peninsula, with fluxes large enough to dominate the domain average. For example, on day 302 (29 October), the average zonal momentum flux over the whole domain is -1.88 mPa, and the contribution from the Peninsula accounts for -1.45 mPa. The contribution from the oceanic region is -0.36 mPa. Such episodes last a day or a few days, and are separated by periods of very weak fluxes. This behaviour contrasts with that of fluxes over the Southern Ocean: the

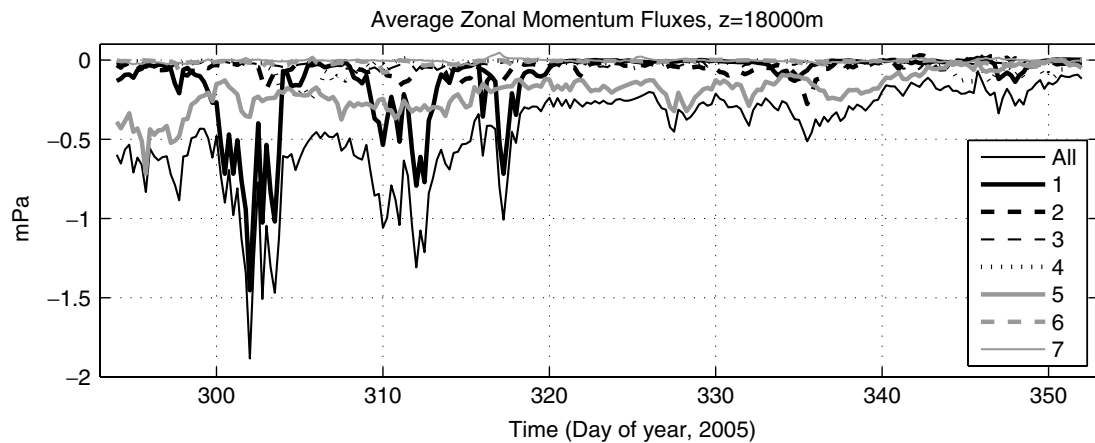


Figure 7. Time series of the zonal momentum fluxes averaged over the whole domain (thin black curve), and of the contributions from the seven different regions shown in Figure 5.

time series is much smoother, without bursts similar to those found over the Peninsula, but also without periods of very weak fluxes. On only a few occasions (e.g. day 296, 23 October) does a significant fluctuation for fluxes in region 5 appear which contributes significantly to a conspicuous fluctuation of the domain average. Of course, this smoothness is in part due to the size of this region, implying a spatial average over many events and hence a smoothing of any local bursts. Yet, this absence of episodic fluctuations equivalent to those over region 1 does rule out that there can be, over the Ocean, intense local events comparable to orographic waves, which could dominate the domain average.

4.2. Intermittency

The momentum fluxes due to GWs are known to vary significantly in time, similar to a succession of events or bursts rather than a smoothly modulated function of time. As emphasized in recent efforts to construct a global picture of the atmospheric GW field (Alexander, 2010), it is important to quantify this intermittency: mean values of the fluxes are not sufficient information for constraining the momentum fluxes in global models. Often, so-called intermittency factors are present in parametrizations to account for the fact that GWs are not present all of the time (e.g. Scinocca and McFarlane, 2000), but they are tunable parameters.

In a similar vein, Plougonven *et al.* (2008) questioned the representativeness of a case-study of a large-amplitude wave event over the Antarctic Peninsula (local fluxes of a few Pa), and found that conditions were *a priori* met for such events 10% of the year. Such events, rare but extremely large, may account for a very large contribution to the mean fluxes. Hence the mean, even complemented by a standard deviation, is not sufficient information. The issue is rather to determine whether rare but very large events contribute significantly to the mean. An appropriate tool to investigate this is the probability distribution function (pdf) of the absolute momentum fluxes (Alexander *et al.*, 2010), the latter being always positive. Investigation of these from balloon and satellite observations and mesoscale simulations show that the pdfs are often close to log-normal (Hertzog *et al.*, 2012). However, over mountainous regions they depart from log-normal distributions to

have larger tails (more frequent extreme events), making the two first moments of the distribution insufficient to describe it. Below, we analyze the intermittency of the wave field and propose a new diagnostic for this purpose.

Recently Hertzog *et al.* (2008) have proposed two diagnostic measures of intermittency based on balloon measurements. One, following Bühler (2003), applies to the description of a source that would always emit with the same amplitude but would have ‘on’ and ‘off’ phases. The other is the ratio of the 50th percentile to the 90th percentile of the fluxes. The latter is more adapted to GWs, which have no reason to have a preferred amplitude. However, the choice of particular percentiles is arbitrary, and the resulting distribution will be quite sensitive to the sampling.

Hence we seek a new diagnostic which would quantify the importance of rare but very large events to the average flux, but would be more robust relative to sampling. It is insightful here to use examples. Say we have N values (measurements or simulation outputs) of fluxes, f_n with $1 \leq n \leq N$, and assume they have been sorted in increasing order ($f_n \leq f_{n+1}$ for all n). Let us now define the cumulative sum of these fluxes:

$$F_n = \sum_{i=1}^n f_i, \quad (1)$$

and note the average $\bar{f} = F_N/N$. A time series having no intermittency at all would be one with a constant value: $f_n = \bar{f}$. In that case, $F_n = n\bar{f}$. The most intermittent time series would have only null values ($f_n = 0$ for $n \leq N-1$) except one single non-zero event ($f_N = N\bar{f}$). Intermediate cases are illustrated in Figures 8 and 9, showing absolute momentum fluxes from the simulations over two locations as time series, and once they are sorted into increasing order (Figure 9(a)). The corresponding cumulative sums are shown in Figure 9(b). The straight diagonal line corresponding to the absolutely not intermittent case ($F_n = n\bar{f}$) is also shown. The most intermittent series would yield an integral that is zero up to the last sampling point, which accounts for the whole sum. A real series will have a behaviour in between, and the area between the diagonal and the cumulative sum of the sorted fluxes provides a

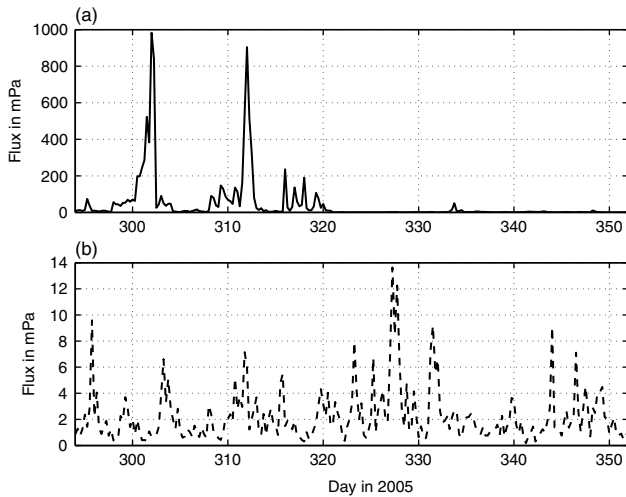


Figure 8. Time series for absolute momentum fluxes at (a) 70.1°S, 63.4°W and (b) 55.7°S, 75.3°W. (The two locations are shown in Figure 10(d).)

measure of the intermittency of the fluxes:

$$I_g = \frac{\sum_{n=1}^{N-1} (n\bar{f} - F_n)}{\sum_{n=1}^{N-1} n\bar{f}}. \quad (2)$$

It is normalized so as to have value 1 for the most intermittent series, and 0 for the constant series.

This measure is very well known in economics and is used to quantify inequalities of income; it is the Gini coefficient (Gini, 1912). We propose this as a measure of intermittency, with the advantage that it does not require an arbitrary choice of a percentile, and it involves integration and hence is not very sensitive to sampling.

Figure 10 compares the intermittency calculated as in Hertzog *et al.* (2008), and quantified with the Gini coefficient. In order to compare with the estimates from balloon observations (Figure 8 in Hertzog *et al.*, 2008), the same grid is used in the left column. Striking features are as follows: the two distributions are very similar, highlighting mountainous regions as the most intermittent, in particular the Antarctic Peninsula (the average over region 1 is 0.63, the maximum value in a $5^\circ \times 10^\circ$ box is 0.79, minimum is 0.45). Some parts of the coastline also have significant intermittency. The greatest parts of the Southern Ocean have relatively low values of intermittency, with no apparent spatial structure (average is 0.44, maximum is 0.58, minimum is 0.34). Only one region within the Southern Ocean stands out with relatively strong intermittency, between 150°W and 90°W, and between 65°S and 55°S—in the southeast Pacific. Inspection of the flow reveals that the values found for the mean fluxes in this specific region (cf. Figures 3 and 4) are due to one intense event, at the beginning of the period (days 296–298, 23–25 October), which also accounts for the small peak found at those dates in Figure 7.

In order to assess whether any spatial structure is present in these estimates of intermittency, other than the distinctions outlined above, the intermittency has been calculated from the momentum fluxes described on the WRF grid (Figures 10(b,d)). Momentum fluxes were calculated as described in section 3.1, but smoothed at each time with

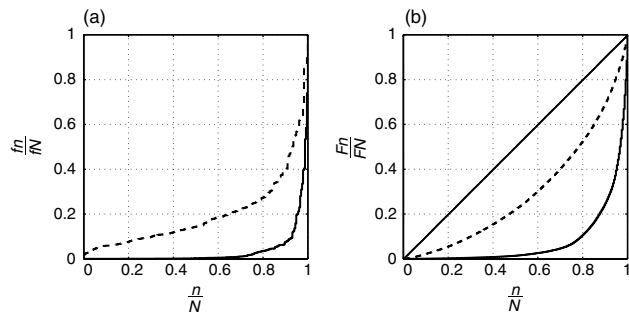


Figure 9. (a) Values of absolute momentum fluxes sorted in increasing order and rescaled by their maximum, for the same locations as Figure 8 (solid line for the Antarctic Peninsula, dashed line for the Southern Ocean). (b) Cumulative sum of the sorted momentum fluxes, rescaled by the sum (the Lorenz curve). The straight line would correspond to a constant process. The intermittency is defined as twice the area between the straight line and the curve of the cumulative sum.

a smoothing window of width 500 km. One could have expected a signature of the background winds to come out. This is not the case. In fact, the intermittency diagnostic covers a significant range of values, but shows little large-scale structure other than the distinction between OGWs and NGWs. Fairly large values of intermittency are clearly associated with South Georgia Island, already highlighted as a potentially important source of waves (Alexander *et al.*, 2009). Over the oceans, intermittency is patchy, and local maxima appear to be contingent and due to specific events of our short period rather than to climatological features.

4.3. Hovmöller diagrams

A synthetic view of the above results regarding both geographical distribution and temporal variability is provided by Hovmöller diagrams. The zonal momentum fluxes are here revisited in this way.

Figure 11 shows a time–latitude view of the simulated zonal momentum fluxes at $z = 17$ km. Three obvious features can be seen:

- (i) The maximal values occur in the latitude range from 65° to 75°S, corresponding to the Peninsula. These maxima are intermittent and mostly confined to the beginning of the period (days 294–318, i.e. 21 October to 14 November 2005), corresponding to very intermittent orographic waves.
- (ii) The region north of 65°, mostly corresponding to the oceans, exhibits moderate fluxes with a much smoother distribution. The smoother distribution is partly due to averaging events over a much wider region, whereas the orographic wave events which dominate the average around 70° are due to a single, narrow region. Again, we note the general decay with time of the fluxes for this latitude band, consistent with Figure 7.
- (iii) Fluxes over the southernmost latitudes are extremely small, corresponding to the very weak values found over the Plateau.

The average over time of such Hovmöller diagram helps to quantify the relative contributions of the OGWs over the Peninsula and the NGWs over the Southern Ocean, as in Hertzog *et al.* (2008). For that purpose, Figure 12 shows the zonal average of the *total* momentum fluxes

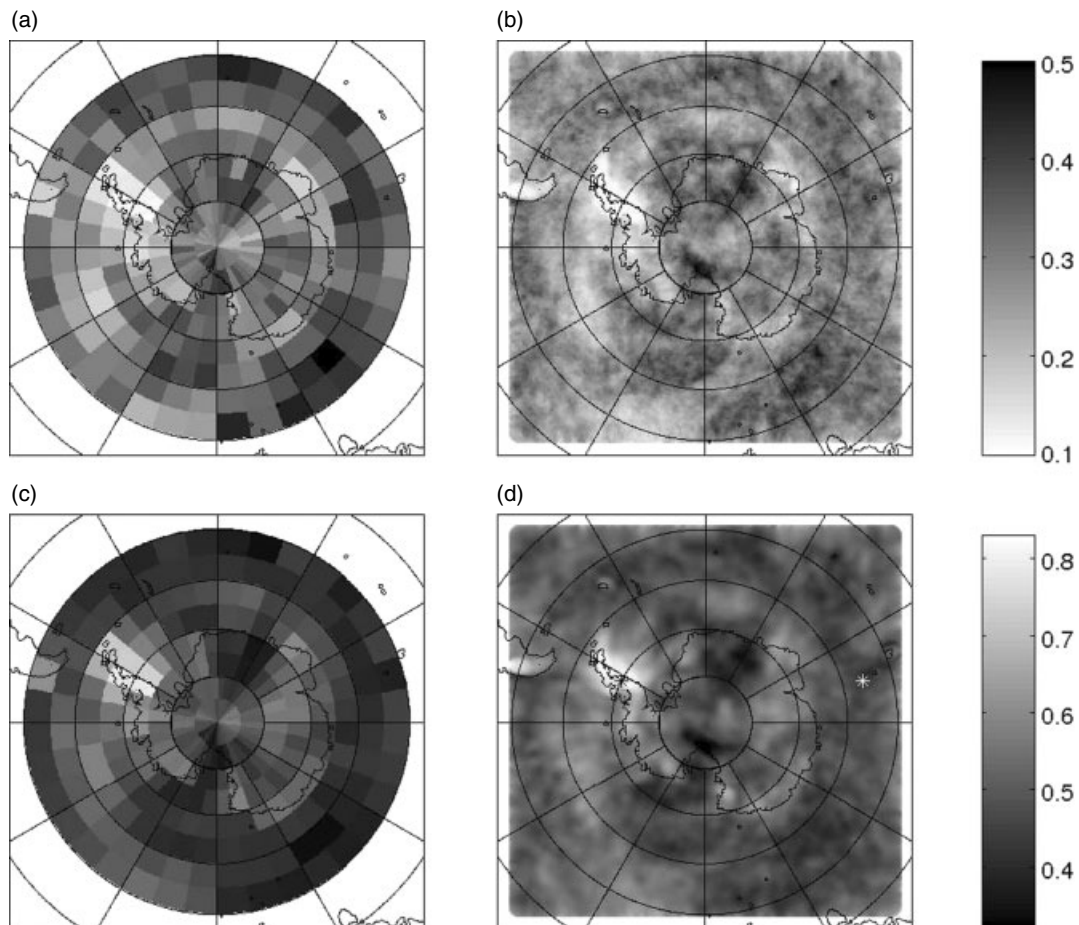


Figure 10. Intermittency of the absolute momentum fluxes estimated from 6 h output of the simulations using (a, b) the Hertzog diagnostic (ratio of 50th to 90th percentile) and (c, d) the Gini coefficient. In (a, c), the calculation uses fluxes averaged in boxes 10° longitude \times 5° latitude. In (b, d), spatially smoothed fluxes at each time interval are used (smoothing window of width 500 km). In (d), the locations used for Figures 8 and 9 are indicated (white * in the Southern Ocean, and black * over the Peninsula).

$(\sqrt{(u'w')^2 + (v'w')^2})$. The average for the whole domain is shown, as well as the contributions from orographic and non-orographic regions (regions 1–4 and 5–7 respectively). Relative to the similar figure obtained from balloon observations (Figure 7 of Hertzog *et al.*, 2008), the overall values are comparable, but there are some differences in the relative importance of OGWs and NGWs: in contrast to the observations, the maximum of fluxes due to OGWs is slightly larger than the maximum of fluxes due to NGWs. This is a consequence of the fact that the simulations overestimate the OGWs and underestimate the NGWs, relative to the balloon observations. Nevertheless, the conclusion emphasized by Hertzog *et al.* (2008) holds: although OGWs clearly account for the largest local values of momentum fluxes, their overall contribution to momentum fluxes entering the stratosphere is comparable with those due to NGWs. The latter are more ubiquitous, have non-zero phase speeds, and care should be taken to quantify them well, although they do not yield locally spectacular values of momentum fluxes.

Figure 13 shows the time–longitude variations of zonal momentum fluxes. The average along meridians was taken between latitudes 50 and 80° S. Again, a very clear signature can be seen for the Antarctic Peninsula, consisting of a narrow band of intermittent, more intense values around 60° W. The novel feature which comes out is the contrast between this spatially fixed source and the propagating

streaks found at other longitudes, corresponding to non-orographic wave sources over the oceans. Intense values of momentum fluxes propagate coherently with speeds comparable to those of baroclinic disturbances (i.e. around 15 m s^{-1}). This speed becomes smaller at the end of the period, i.e. at the end of spring. The temporal width of these streaks is of only a day or two. Some interactions can sometimes be seen with the Peninsula, e.g. the large values at days 296–298 (23–25 October), near 100° W which come onto the Peninsula just prior to a major episode of OGWs (days 300–305). In short, the Hovmöller diagram in Figure 13 provides evidence that the NGWs above the oceans are emitted by jets and fronts and move with those, consistent with the picture that has emerged from idealized numerical simulations of emitted waves attached to the flow features (source, jet exit region) at the origin of the waves (Plougonven and Snyder, 2007). To support this interpretation, Figure 14 shows a Hovmöller diagram of the meridional wind in the upper troposphere ($z = 9 \text{ km}$), as a crude indication of synoptic activity in the troposphere. We find an eastward propagation at speeds consistent with the propagation speeds found for momentum fluxes in the lower stratosphere. Several of the local maxima in the momentum fluxes at 18 km can be seen to coincide with conspicuous signals in the tropospheric synoptic activity, but this is not systematic. Further investigation will be required

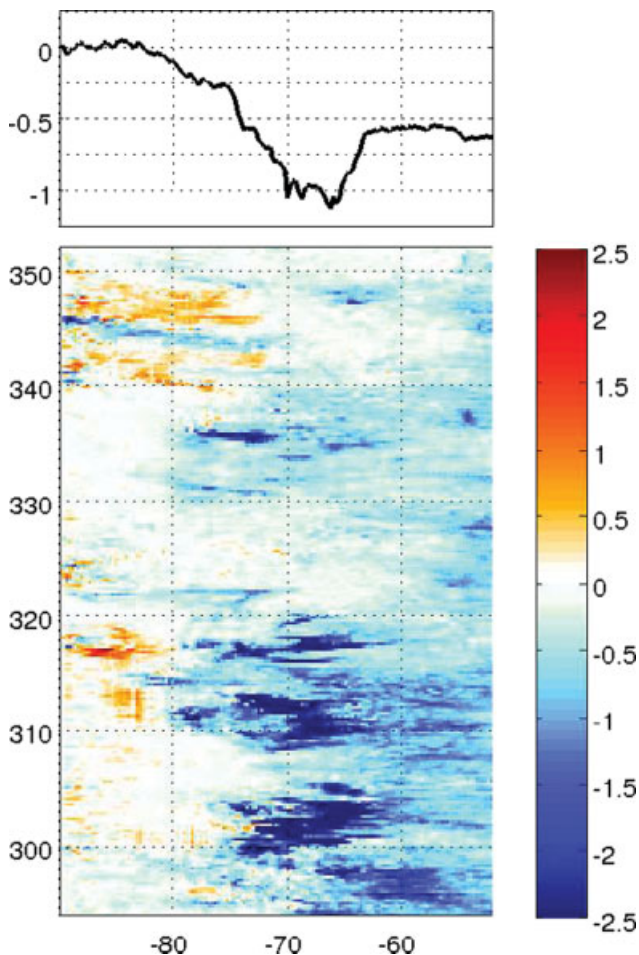


Figure 11. (b) shows the Hovmöller diagram of zonal momentum fluxes (mPa) averaged zonally, at $z = 18$ km. The vertical axis shows time (day of year) and the horizontal axis shows latitude. (a) shows the time average over the whole period of the zonally averaged fluxes.

to relate the tropospheric flow and the lower-stratospheric GWs more precisely.

5. Vertical structure of the GW field

The simulations make it possible to explore the global structure of the wave field. In the present study we only briefly investigate the vertical variations of the GW field, motivated by two specific questions. One is to determine how representative is the wave field observed at the precise set of heights set by the balloon flight levels. The other is to obtain insights regarding the effect of the GW field on the background flow in the lower stratosphere.

Figure 15 shows the time-averaged zonal momentum fluxes at four evenly spaced heights between 10 and 25 km. The calculation and presentation are the same as in Figure 3. Quite strikingly, the overall structure of the wave field changes significantly in the first kilometres of the stratosphere, between 10 and 15 km. In contrast, above the altitude of 15 km, the spatial pattern does not change but the absolute values decrease. The mean of the absolute value of zonal momentum fluxes decreases from 20 mPa at 10 km to 4 mPa at 15 km, to 1.2 mPa at 20 km, and finally 0.4 mPa at 25 km.

Above the oceans, these plots (for $z > 15$ km) also suggest the concentration of larger momentum fluxes in regions where the jet associated with the polar vortex is present.

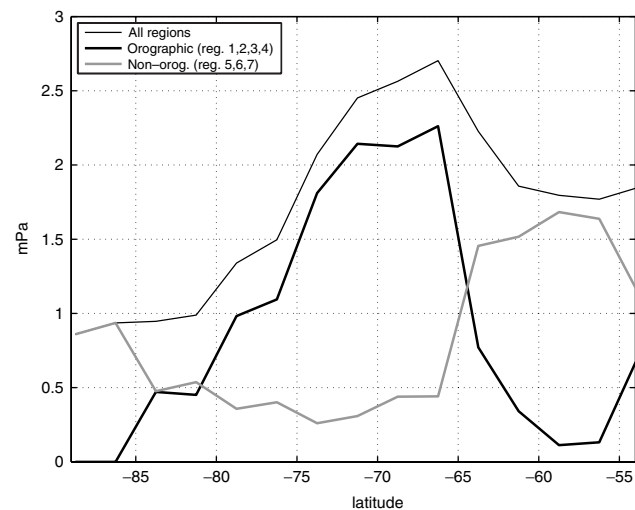


Figure 12. Zonal average of the total momentum fluxes (mPa), poleward of 52°S , as a function of latitude. The thin black curve shows the average over the whole domain, and the bold curves show the contribution from orographic regions (black) and from non-orographic regions (grey).

This positive correlation between large background wind speed and momentum fluxes is consistent with arguments expected from propagation (Dunkerton, 1984), and with analysis of recent high-resolution GCM studies (Sato *et al.*, 2009). Arguments based simply on the linear theory of wave propagation in a background flow indeed show that horizontal propagation will tend to focus waves toward the core of the jet; the positive shear on the southward side of the jet modifies the meridional wavenumber in such a way as to inhibit outward propagation from the core of the jet. Ray-tracing calculations by Dunkerton (1984) and Sato *et al.* (2009) confirm and illustrate this.

At $z = 10$ km, the distribution differs strongly^{||} from those above; there are significant areas of positive values around the coastline of Antarctica where the surface winds descending from the Plateau are deflected by the Coriolis force as easterlies. This thus suggests a strong generation of GWs by katabatic winds and their dissipation in the lower stratospheric westward shear. Above the oceans, there are regions of enhanced negative fluxes (e.g. around 60°E and 140°E) which may indicate an inhomogeneity of the wave sources. Yet both of these features (positive values around the coastline, and local enhancements above the oceans) disappear at $z = 15$ km. Now, a flux of 5 mPa dissipated between 10 to 15 km can be equivalent to an acceleration of $0.3 \text{ m s}^{-1} \text{ day}^{-1}$. This implies significant forcing in the first kilometres of the stratosphere, especially a drag on the westerly winds above the coastline.

The similarity of the spatial pattern of fluxes at different heights of the lower stratosphere (15, 20, 25 km) and their dissimilarity with the map of fluxes at 10 km also suggests that the inhomogeneity of the non-orographic sources (at $z = 10$ km) may fade away quickly. It also strengthens conclusions from previous studies advising to choose a launch level at the top of the troposphere for parametrizations (Manzini and McFarlane, 1998; Ern *et al.*, 2006).

^{||}One should interpret this with some caution. At this height, the spatial filtering will not only isolate GWs, but also upper-level fronts.

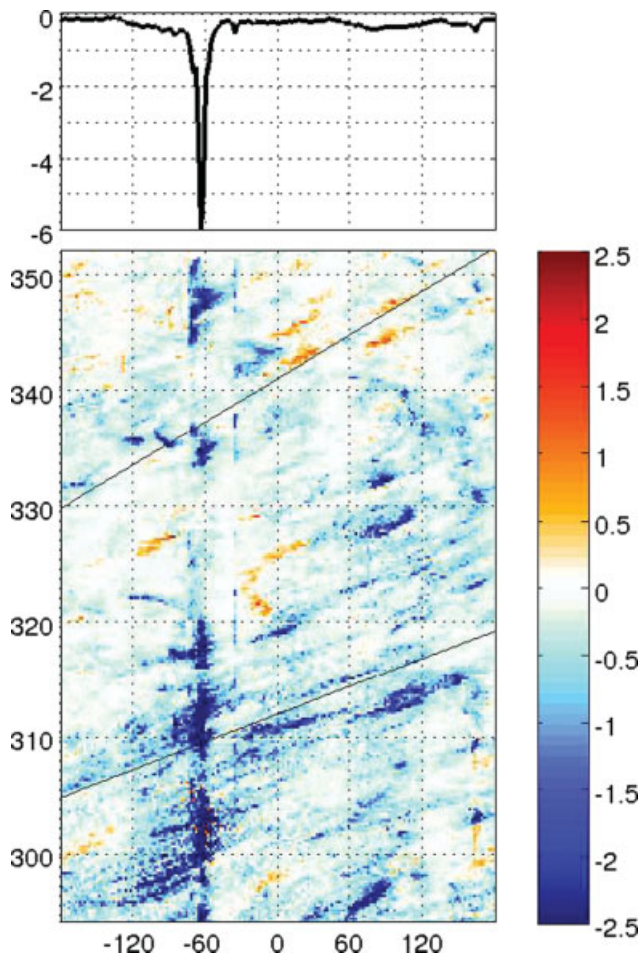


Figure 13. As Figure 11, but averaged meridionally between 52° and 80° S. Also indicated are two lines corresponding to propagation speeds of 16 m s^{-1} (around day 310) and 10.3 m s^{-1} (around day 340).

6. Sensitivity of the numerical results

It is known that simulated GWs are particularly sensitive to resolution, and this has been analyzed in detail for orographic waves (Smith *et al.*, 2006), convective waves (Lane and Knievel, 2005) and waves forced by jets and fronts (Zhang, 2004; Plougonven and Snyder, 2007). Hence we focus below on the sensitivity of our results to resolution (section 6.1), but we also take advantage of the experiment design to analyze the sensitivity to the length of the simulation (section 6.2).

6.1. Sensitivity to resolution

The sensitivity to resolution was investigated by simulations over the same domain but with doubled horizontal resolution ($\Delta x = 10 \text{ km}$). The vertical resolution was left unchanged as previous work showed that the resulting GWs were not very sensitive to it (Plougonven and Snyder, 2007; Plougonven *et al.*, 2010). These simulations are expected to resolve waves down to wavelengths 60–100 km (Skamarock, 2004), i.e. shorter than the shortest wavelengths generally visible by the balloons (Hertzog *et al.*, 2008).

Three simulations at double horizontal resolution have been run for periods which were chosen because they contained significant GW events over the ocean (23–26 November, 25–28 November, and 5–8 December 2005). As

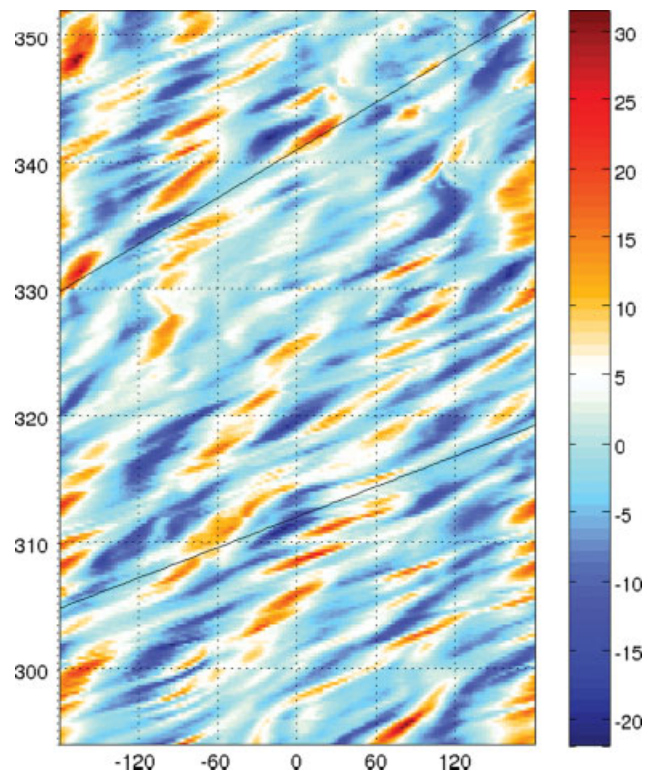


Figure 14. Hovmöller diagram similar to Figure 13, but for the meridional wind at height 9 km, averaged meridionally between 52° and 65° S. The same two lines corresponding to propagation speeds of 16 m s^{-1} and 10.3 m s^{-1} are shown for reference.

an example of the fine detail present in the high-resolution simulations, Figure 16 shows the vertical velocity field in one quarter of the domain (longitudes 0 to 90° E), to be compared with Figure 2. Some islands are present, and have an intense GW signature, but most of the GWs present are due to fronts and jets over the ocean. More generally, over the six days simulated at both resolutions, the same structure of the GW field is reproduced at higher resolution but with sharper details and enhanced amplitudes. The vertical velocity is typically larger by a factor of about 1.6. The small-scale part of horizontal velocities are only slightly increased (by a factor of about 1.1).

The fluxes have been calculated in the high-resolution simulations and compared with those from the standard simulations. A filtering window of 1000 km has been used for both, and the comparison is carried out at 18 km height. Again the comparison can be carried out for the time average, over the six simulated days available, and for fluxes at individual times, every 6 h. Figure 17 shows the comparison of the time-averaged zonal momentum fluxes. Remarkably, the spatial patterns obtained for these fluxes is insensitive to resolution: only minor differences between the two can be identified in the spatial variations. The values, on the other hand, increase by a factor slightly less than 2. This ratio is slightly larger for OGWs than for NGWs, consistent with a strong effect from the better resolved orography. Figure 18 shows a more stringent test, i.e. a scatterplot of instantaneous zonal and meridional fluxes. The values calculated from the runs with standard resolution are found to correlate very well with those from the high-resolution runs (correlation coefficient of 0.81 for zonal momentum fluxes, 0.86 for meridional fluxes). A linear regression yields a slope of 1.6 for zonal momentum fluxes, and 2.1 for meridional fluxes.

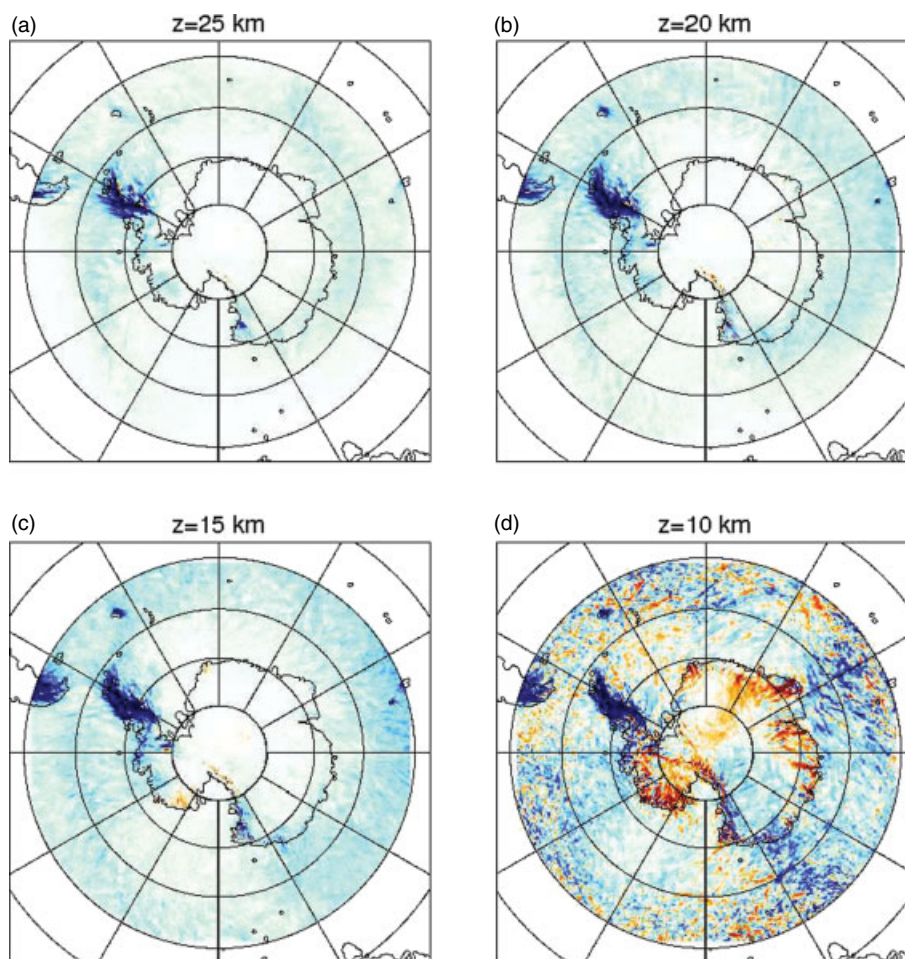


Figure 15. Zonal momentum fluxes at (a) $z = 25$ km, (b) $z = 20$ km, (c) $z = 15$ km and (d) $z = 10$ km. Colours range from -5 mPa to 5 mPa, as in Figure 3.

This likely reflects the importance of orographic waves along the coast of Antarctica in the meridional fluxes.

In conclusion, the thorough examination of the GW field, quantified by the momentum fluxes, confirms the conclusion suggested from visual comparison of Figures 2 and 16: the simulation contains finer detail and slightly larger amplitudes (factor 1.5 to 2) at higher resolution, but the structure of the wave field is unchanged. This provides strong evidence that the simulations with $\Delta x = 20$ km and $\Delta z = 300$ m give robust information about the GW field's spatial variations, and good indications regarding its amplitudes. It also suggests, as expected, that the standard simulations underestimate the amplitudes. Nonetheless, one needs to be wary of holding higher resolution as the truth; increasing the resolution does not necessarily only improve the realism, and we are still far from a resolution that would include all processes (Lane and Knivvel, 2005).

Since the momentum fluxes obtained from 'standard' simulations were globally consistent with the balloon observations, the high-resolution simulations therefore also provide momentum fluxes that are typically twice as large as the balloon estimates. As discussed in Hertzog *et al.* (2008), this underestimation of the Vorcore fluxes can be explained by two factors. First, the Vorcore balloons only resolve waves with an intrinsic period longer than 1 h. Based on the $\widehat{\omega}^{-1}$ dependence of the momentum-flux spectrum, Hertzog *et al.* (2008) estimated that about half of the momentum flux could be carried by waves with intrinsic periods shorter

than 1 h, i.e. the balloon observations underestimate the total flux by a factor of 2. Second, the detection of GWs in the balloon dataset is limited by the presence of noise in the measurements, which typically contributes to losing another $\sim 15\%$ of the total flux. This is more pronounced for higher intrinsic frequencies (up to $\sim 50\%$ for the highest-frequency waves ($2\pi/\widehat{\omega} \sim 1$ h), the contribution of which is likely to be higher over orography).

In summary, the different sets of simulations and observations are narrowing down towards robust and consistent values of momentum fluxes. The present balloon dataset and simulations provide estimates that vary within a factor two, with different biases for OGWs and NGWs. Several approaches will contribute to a more conclusive determination of the absolute amplitude of the momentum fluxes: case-studies based on the above simulations and observations will help compare in detail the small-scale perturbations in the simulations and the observations, further simulations with higher resolution, and new observations (Rabier *et al.*, 2010) with a higher sampling rate so as to resolve the whole GW spectrum.

6.2. Sensitivity to the length of the simulation

The sensitivity of the computed momentum fluxes to the length of the simulations is tied to the predictability and the choice of the spin-up time. In this preliminary work to set up these simulations (Plougonven *et al.*, 2010), tests were

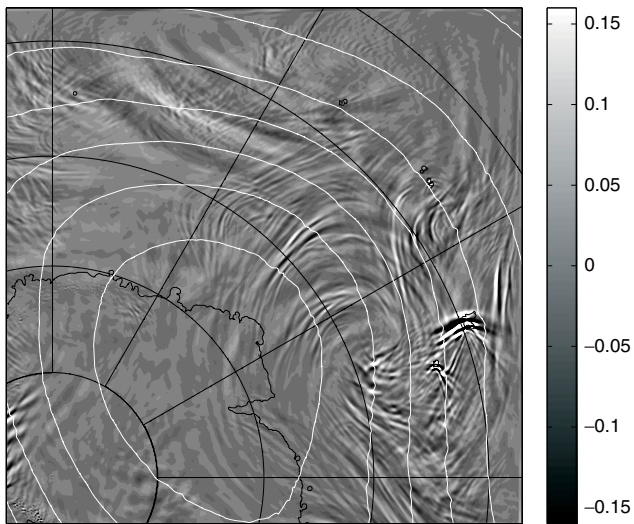


Figure 16. As Figure 2(b), but from a simulation with doubled horizontal resolution ($\Delta x = 10$ km).

carried out to determine what the appropriate length of the simulations should be: how long need the spin-up be, and how long do the simulations remain close enough to the real flow for a relevant comparison with the balloons? The second question concerns the predictability of the flow, and more specifically of the GW field in the lower stratosphere. The present simulations give us an excellent opportunity to revisit these issues, more systematically than in a simple case-study.

For each of the 28 first simulations, the third day overlaps with the first day of the following simulation. We compare the GW field at the final time (after three simulated days) of a simulation with its equivalent in the following simulation (after one simulated day).

Scatterplots of zonal momentum fluxes estimated after 24 h of simulation versus those estimated after 72 h have been investigated (not shown). The correlation coefficient between the two sets of values is 0.72. When focusing on specific regions, the correlation is between 0.70 and 0.75, with slightly smaller values for the ocean. The average of the absolute value of the momentum fluxes after 72 h is larger by about 12% than the equivalent after 24 h. This is consistent with the expectation that the GW field develops during the simulation, but rather shows that this is marginal. This small difference confirms, *a posteriori*, the choice of 24 h as an appropriate spin-up time for investigations of the GW field. Moreover, this gives us an order of magnitude of the error bar associated with sensitivity to the length of the simulation, i.e. 10–15%.

7. Summary and discussion

The GW field in the lower stratosphere over Antarctica and the Southern Ocean has been investigated using meso-scale simulations and balloon observations. The balloon observations from the Vorcore campaign (Hertzog *et al.*, 2007) provide a unique database of *in situ* measurements well adapted to quantifying GWs, with a large spatial and temporal coverage. The simulations were run with the WRF model, with a resolution of $\Delta x = 20$ km and 120 levels in a domain $10\,000 \times 10\,000$ km centred on the Pole. 58 simulated days, from 0000 UTC on 21 October to 0000 UTC on 18 December, were analyzed.

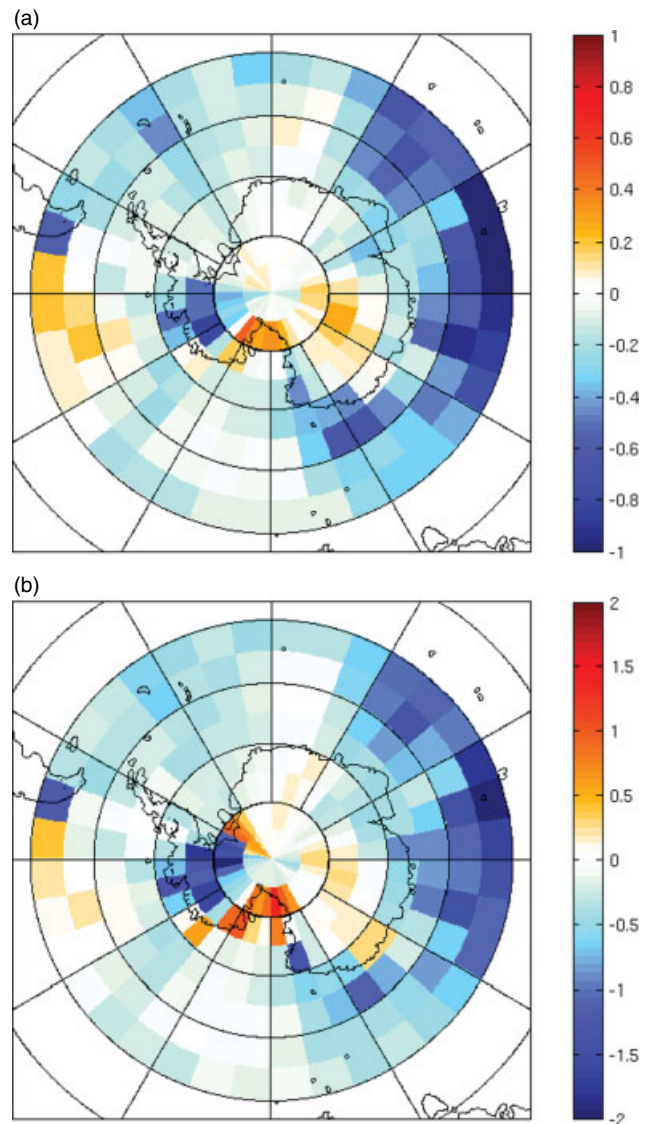


Figure 17. Time average of the zonal momentum fluxes (mPa) at $z = 18$ km for (a) the standard simulations, and (b) the high-resolution simulations. The time average covers 6 days. The colour range is doubled for the high-resolution results.

The two main objectives of this study were (i) to assess the realism of the simulated GW field by comparison with the balloon observations, and (ii) to describe and quantify further the GW field based on the simulations.

The comparison between simulations and observations focused on momentum fluxes, because of the need for constraints for modelling purposes (Alexander *et al.*, 2010) and because this was the main quantity analyzed from the balloon observations (Hertzog *et al.*, 2008). The momentum fluxes were calculated at the heights of the balloons, in the lower stratosphere, i.e. $17 < z < 19$ km. The GW field results from contributions from different source mechanisms, and it is most relevant to separate orographic GWs (OGWs) and non-orographic GWs (NGWs). To characterize waves from these different sources, the domain was decomposed into seven regions. Analysis focused on two in particular: the Antarctic Peninsula (for OGWs) and the Southern Ocean (far from coastlines and islands, for NGWs). The comparison yields the following conclusions:

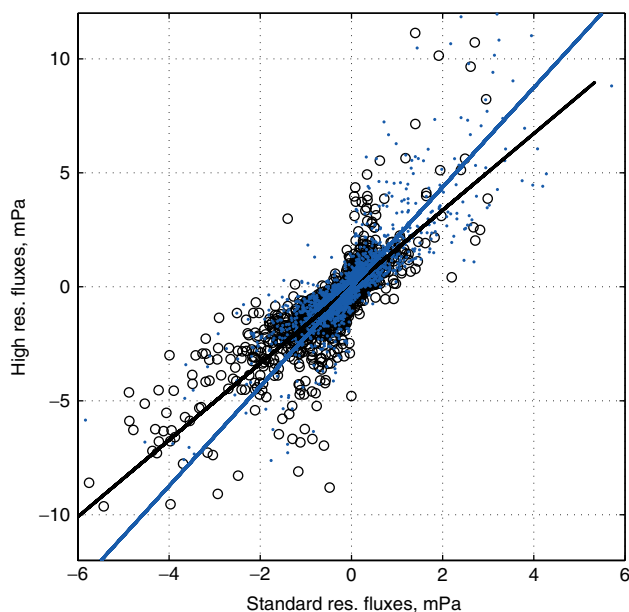


Figure 18. Scatterplot and linear regressions for instantaneous values of standard (horizontal axis) and high-resolution (vertical axis) fluxes; zonal (circles) and meridional (dots) momentum fluxes are averaged over $10^\circ \times 5^\circ$ boxes, at $z = 18$ km. Regression slopes are 1.6 (black line, zonal momentum fluxes) and 2.1 (meridional momentum fluxes). This figure is available in colour online at wileyonlinelibrary.com/journal/qj

1. There is a satisfactory agreement overall between the simulated and the observed zonal momentum fluxes. The overall time average, using the sampling by the balloons, is -0.90 mPa from the balloons, and -0.92 mPa from the simulations.
2. The agreement between simulations and observations strongly varies between the regions. Relative to the observations, the model overestimates OGWs (by a factor ~ 2.5 above the Peninsula), but underestimates NGWs (by a factor ~ 0.8). Hence, the contrast between locally strong OGWs and weak NGWs is exacerbated in the simulations relative to the observations.
3. The time averages over this period are sensitive to the limited sampling of the balloons. This mainly reflects the temporal bias toward the beginning of the period, when fluxes were more intense and more observations were available.
4. Zonal momentum fluxes over Drake Passage have similar values to the nearby 'hot spot' orographic regions in the observations, but much weaker values in the simulations, closer to the oceanic values. It confirms that the simulations are not capturing well the GW wakes surrounding major topographic obstacles, as already pointed out in Plougonven *et al.* (2010).
5. The Antarctic Plateau has zonal momentum fluxes one order of magnitude lower than over the oceans, very consistently in both the observations and simulations.
6. The simulations and observations do not provide evidence of a significant enhancement of GW momentum fluxes over the islands of the Southern Ocean, but this may simply reflect insufficient sampling and an unfavourable time period.
7. Meridional momentum fluxes show less agreement than zonal ones. However, some robust features emerge: fluxes are strong and equatorward over the

Peninsula, and they are weaker and poleward over the ocean. The overall average is poleward, though much weaker in the simulations than in the observations.

One of the conclusions of Hertzog *et al.* (2008) was that, although OGWs dominate fluxes by their huge local values over the Peninsula, the integrated contribution of fluxes over the regions corresponding to NGWs was at least as strong, or even stronger. In the simulations, the contrast between OGWs and NGWs is enhanced, due to the relative overestimation of the former and underestimation of the latter. Yet the conclusion holds that the integrated contributions from NGWs are comparable to those from OGWs.

The simulations provide a more complete view of the GW field than the sporadic sampling of the balloons, making it possible to better describe the variability of the GW field. Time series of the zonal momentum fluxes in the different regions revealed different temporal variability, with OGWs exhibiting very strong intermittency (alternation of quiet periods and periods with very intense values which dominate by several orders of magnitude the fluxes in the whole domain). This added to previous motivation (Hertzog *et al.*, 2008; Plougonven *et al.*, 2008; Alexander *et al.*, 2010) to try and quantify the intermittency of the GW field. A new measure of intermittency, the Gini coefficient, was introduced. Used in economics to quantify inequalities of income, it has the advantage of being free of arbitrary choices, and straightforward to compute from a finite sample of values. Values of intermittency thus defined typically vary between 0.3 and 0.8, the largest values being found near orography (0.6–0.7), in particular the Peninsula. Aside from the strong contrast between orographic and oceanic regions, remarkably little large-scale structure comes out. As OGWs and NGWs are handled by different parametrization schemes, the present analysis of intermittency may hence provide a general estimate for NGWs at high latitudes (0.4–0.5), but no clear information on a spatial structure for this quantity.

Most of the above conclusions are well summarized in Hovmöller diagrams (section 4.3). The longitude–time diagram in particular very clearly reveals the distinction between the different types of sources contributing to the GW field: a fixed stationary source at the longitude of the Peninsula emits intermittent bursts of waves, mostly in the first half of the period (20 October–14 November 2005). The other contribution to the GW field comes from weather systems propagating at phase speeds ~ 15 m s $^{-1}$ over the oceans.

The variation with height was investigated, and revealed significant differences between the fluxes near the tropopause ($z = 10$ km) and in the lower stratosphere (15, 20, 25 km). The spatial pattern hardly changes at those latter heights, with a maximum over the Peninsula, and weaker but locally enhanced values along the stratospheric jet. One conclusion is that the observations from balloons describe a spatial distribution of fluxes that is representative for a broad range of heights. Near the tropopause, the structure of the fluxes differed, with conspicuous maxima (positive fluxes of zonal momentum) above the Antarctic coastline. These disappear in the first kilometres of the stratosphere and contribute there to a drag on the westerlies.

The sensitivity of the results to different aspects of the model configuration were investigated. A major finding is that, although the GW amplitudes remain sensitive

to resolution (when the resolution is doubled in the horizontal ($\Delta x = 10$ km), momentum fluxes are multiplied almost by ~ 2), the spatial structure of the GW field is not. This is evidence that the simulations with moderate resolution ($\Delta x = 20$ km) provide valuable information on the variability of the GWs, while globally underestimating their amplitudes. A caveat is that the period chosen for the high-resolution simulations did not include significant OGWs over the Peninsula. The sensitivity to the length of the simulation was also tested, showing a mild sensitivity for the average fluxes.

The present study is key to demonstrating the satisfactory realism of these simulations, and provides a first analysis of the GW field in these simulations. Further work will include case-studies which will help determine why there are discrepancies between the simulations and observations for individual events (especially for NGWs, as Plougonven *et al.* (2008) and other such case-studies already provide insight regarding OGWs), and identification of source mechanisms. Another direction for further use of the present simulations is the systematic investigation of the non-orographic sources of waves above the oceans.

Acknowledgements

The authors are grateful to Andreas Dörnbrack and an anonymous reviewer for helpful and constructive comments and suggestions which improved the manuscript. This work received support from LEFE project InDySC. This work was granted access to the HPC resources of [CCRT/CINES/IDRIS] under the allocation 2009-012039 and 2010-012039 made by GENCI (Grand Equipement National de Calcul Intensif) The authors would like to acknowledge the French Space Agency (CNES) as well as the NSF for their long-standing support of the Vorcore campaign. The Laboratoire de Météorologie Dynamique is a member of the Institut Pierre Simon Laplace.

References

- Alexander MJ. 2010. 'A report on the SPARC gravity wave activity'. *SPARC Newsletter* **35**: 17–18.
- Alexander MJ, Teitelbaum H. 2007. Observation and analysis of a large-amplitude mountain wave event over the Antarctic Peninsula. *J. Geophys. Res.* **112**(D21103): DOI: 10.1029/2006JD008368.
- Alexander MJ, Eckermann S, Broutman D, Ma J. 2009. Momentum flux estimates for South Georgia Island mountain waves in the stratosphere observed via satellite. *Geophys. Res. Lett.* **36**(L12816): DOI: 10.1029/2009GL038587.
- Alexander MJ, Geller M, McLandress C, Polavarapu S, Preusse P, Sassi F, Sato K, Eckermann S, Ern M, Hertzog A, Kawatani Y, Pulido M, Shaw TA, Sigmund M, Vincent R, Watanabe S. 2010. Recent developments in gravity-wave effects in climate models and the global distribution of gravity-wave momentum flux from observations and models. *Q. J. R. Meteorol. Soc.* **136**: 1103–1124.
- Alexander SP, Tsuda T, Kawatani Y, Takahashi M. 2008. Global distribution of atmospheric waves in the equatorial upper troposphere and lower stratosphere: COSMIC observations of wave–mean flow interactions. *J. Geophys. Res.* **113**(D24115): DOI: 10.1029/2008JD010039.
- Andrews D, Holton J, Leovy C. 1987. *Middle atmosphere dynamics*. Academic Press.
- Austin J, Shindell D, Beagley SR, Brühl C, Dameris M, Manzini E, Nagashima T, Newman PA, Pawson S, Pitari G, Rozanov E, Schnadt C, Shepherd TG. 2003. Uncertainties and assessment of chemistry-climate models of the stratosphere. *Atm. Chem. Phys.* **3**: 1–27.
- Boccara G, Hertzog A, Vincent R, Vial F. 2008. Estimation of gravity-wave momentum fluxes and phase speeds from long-duration stratospheric balloon flights. 1. Theory and simulations. *J. Atmos. Sci.* **65**: 3042–3055.
- Bühler O. 2003. Equatorward propagation of inertia-gravity waves due to steady and intermittent wave sources. *J. Atmos. Sci.* **60**: 1410–1419.
- Doyle J, Shapiro M, Jiang Q, Bartels D. 2005. Large-amplitude mountain wave breaking over Greenland. *J. Atmos. Sci.* **62**: 3106–3126.
- Dunkerton T. 1984. Inertia-gravity waves in the stratosphere. *J. Atmos. Sci.* **41**: 3396–3404.
- Ern M, Preusse P, Alexander M, Warner C. 2004. Absolute values of gravity wave momentum flux derived from satellite data. *J. Geophys. Res.* **109**(D20103): DOI: 10.1029/2006JD007327.
- Ern M, Preusse P, Warner C. 2006. Some experimental constraints for spectral parameters used in the Warner and McIntyre gravity wave parameterization scheme. *Atmos. Chem. Phys.* **6**: 4361–4381.
- Eyring V, Waugh DW, Bodeker GE, Cordero E, Akiyoshi H, Austin J, Beagley SR, Boville BA, Braesicke P, Brühl C, Butchart N, Chipperfield MP, Dameris M, Deckert R, Deushi M, Frith SM, Garcia RR, Gettelman A, Giorgetta MA, Kinnison DE, Mancini E, Manzini E, Marsh DR, Matthes S, Nagashima T, Newman PA, Nielsen JE, Pawson S, Pitari G, Plummer DA, Rozanov E, Schraner M, Scinocca JF, Semeniuk K, Shepherd TG, Shibata K, Steil B, Stolarski RS, Tian W, Yoshiki M. 2007. Multimodel projections of stratospheric ozone in the 21st century. *J. Geophys. Res.* **112**(D16303): DOI: 10.1029/2006JD008332.
- Fritts D, Alexander M. 2003. Gravity wave dynamics and effects in the middle atmosphere. *Rev. Geophys.* **41**: 1003.
- Gini C. 1912. *Variabilità e mutabilità* (Variability and mutability). Reprinted in *Memorie di metodologica statistica*, Pizzetti E, Salvemini, T. (eds) Libreria Eredi Virgilio Veschi: Rome 1955.
- Hamilton K, Wilson R, Hemler R. 1999. Middle atmosphere simulated with high vertical and horizontal resolution versions of a GCM: improvements in the cold pole bias and generation of a QBO-like oscillation in the Tropics. *J. Atmos. Sci.* **56**: 3829–3846.
- Hertzog A, Boccara G, Vincent R, Vial F, Coquerez P. 2008. Estimation of gravity-wave momentum fluxes and phase speeds from long-duration stratospheric balloon flights. 2. Results from the Vorcore campaign in Antarctica. *J. Atmos. Sci.* **65**: 3056–3070.
- Hertzog A, Alexander M, Plougonven R. 2012. On the probability density functions of gravity wave momentum flux in the stratosphere. *J. Atmos. Sci.* submitted.
- Hertzog A, Coquerez P, Guilbon R, Valdivia J-N, Venel S, Basdevant C, Boccara G, Bordereau J, Briot B, Vial F, Cardonne A, Ravissot A, Schmitt E. 2007. Stratéole/Vorcore – Long-duration superpressure balloons to study the Antarctic lower stratosphere during the 2005 winter. *J. Ocean. Atmos. Technol.* **24**: 2048–2061.
- Jones P, Hamilton K, Wilson R. 1997. A very high resolution general circulation model simulation of the global circulation in austral winter. *J. Atmos. Sci.* **54**: 1107–1116.
- Kawatani SWY, Tomikawa Y, Miyazaki K, Takahashi M, Sato K. 2008. General aspects of a T213L256 middle atmosphere general circulation model. *J. Geophys. Res.* **113**(D12110): DOI: 10.1029/2008JD010026.
- Kim Y-J, Eckermann S, Chun H-Y. 2003. An overview of the past, present and future of gravity-wave drag parameterization for numerical climate and weather prediction models. *Atmos.–Ocean* **41**: 65–98.
- Lane T, Knievell J. 2005. Some effects of model resolution on simulated gravity waves generated by deep, mesoscale convection. *J. Atmos. Sci.* **62**: 3408–3419.
- Limpasuvan V, Wu D, Alexander M, Xue M, Hu M, Pawson S, Perkins J. 2007. Stratospheric gravity wave simulation over Greenland during 24 January 2005. *J. Geophys. Res.* **112**(D10115): DOI: 10.1029/2006JD007823.
- Lott F, Fairhead L, Hourdin F, Levan P. 2005. The stratospheric version of LMDz: Dynamical climatologies, Arctic Oscillation, and impact on the surface climate. *Clim. Dyn.* **25**: 851–868.
- Manzini E, McFarlane N. 1998. The effect of varying the source spectrum of a gravity wave parameterization in a middle atmosphere general circulation model. *J. Geophys. Res.* **103**(D24): 31523–31539.
- Morgenstern O, Giorgetta MA, Shibata K, Eyring V, Waugh DW, Shepherd TG, Akiyoshi H, Austin J, Baumgaertner AJG, Bekki S, Braesicke P, Brühl C, Chipperfield MP, Cugnet D, Dameris M, Dhomse S, Frith SM, Garny H, Gettelman A, Hardiman SC, Hegglin MI, Jöckel P, Kinnison DE, Lamarque J-F, Mancini E, Manzini E, Marchand M, Michou M, Nakamura T, Nielsen JE, Olivé D, Pitari G, Plummer DA, Rozanov E, Scinocca JF, Smale D, Teyssède H, Toohey M, Tian W, Yamashita Y. 2010. Review of the formulation of present-generation stratospheric chemistry-climate models and associated external forcings. *J. Geophys. Res.* **115**(D00M02): DOI: 10.1029/2009JD013728.

- Plougonven R, Snyder C. 2007. Inertia-gravity waves spontaneously generated by jets and fronts. Part I: Different baroclinic life cycles. *J. Atmos. Sci.* **64**: 2502–2520.
- Plougonven R, Hertzog A, Teitelbaum H. 2008. Observations and simulations of a large-amplitude mountain wave breaking above the Antarctic Peninsula. *J. Geophys. Res.* **113**(D16113): DOI: 10.1029/2007JD009739.
- Plougonven R, Arsac A, Hertzog A, Guez L, Vial F. 2010. Mesoscale simulations of the gravity wave field above Antarctica during Vorcore. *Q. J. R. Meteorol. Soc.* **136**: 1371–1377.
- Rabier F, Bouchard A, Brun E, Doerenbecher A, Guedj S, Guidard V, Karbou F, Peuch V-H, El Amraoui L, Puech D, Genthon C, Picard G, Town M, Hertzog A, Vial F, Cocquerez P, Cohn SA, Hock T, Fox J, Cole H, Parsons D, Powers J, Romberg K, VanAndel J, Deshler T, Mercer J, Haase JS, Avallone L, Kalnajs L, Mechoso CR, Tangborn A, Pellegrini A, Frenot Y, Thépaut J-N, McNally AP, Balsamo G, Steinle P. 2010. The Concordiasi project in Antarctica. *Bull. American Meteorol. Soc.* **91**: 69–86.
- Sato K, Kumakura T, Takahashi M. 1999. Gravity waves appearing in a high-resolution GCM simulation. *J. Atmos. Sci.* **56**: 1005–1018.
- Sato K, Watanabe S, Kawatani Y, Tomikawa Y, Miyazaki K, Takayashi M. 2009. On the origins of mesospheric gravity waves. *Geophys. Res. Lett.* **36**(L19801): DOI: 10.1029/2009GL039908.
- Sato K, Tateno S, Watanabe S, Kawatani Y. 2012. Gravity wave characteristics in the Southern Hemisphere revealed by a high-resolution middle-atmosphere general circulation model. *J. Atmos. Sci.* **69**: 1378–1396.
- Scinocca J, McFarlane. 2000. The parametrization of drag induced by stratified flow over anisotropic orography. *Q. J. R. Meteorol. Soc.* **126**: 2353–2393.
- Skamarock W. 2004. Evaluating mesoscale NWP models using kinetic energy spectra. *Mon. Weather Rev.* **132**: 3019–3032.
- Skamarock W, Klemp J, Dudhia J, Gill D, Barker D, Duda M, Huang X-Y, Wang W, Powers JG. 2008. *A description of the Advanced Research WRF version 3*. Technical Note. NCAR: Boulder, USA.
- Smith S, Doyle J, Brown A, Webster S. 2006. Sensitivity of resolved mountain drag to model resolution for MAP case-studies. *Q. J. R. Meteorol. Soc.* **132**: 1467–1487.
- Wang W, Bruyère C, Duda M, Dudhia J, Gill D, Lin H-C, Michalakes J, Rizvi S, Zhang X. 2009. 'ARW Version 3 modeling system user's guide'. Mesoscale and Microscale Division, NCAR: Boulder, USA.
- Wu DL, Jiang JH. 2002. MLS observations of atmospheric gravity waves above Antarctica. *J. Geophys. Res.* **107**(4773): DOI: 10.1029/2002JD002390.
- Wu DL, Zhang F. 2004. A study of mesoscale gravity waves over the North Atlantic with satellite observations and a mesoscale model. *J. Geophys. Res.* **109**(D22104): DOI: 10.1029/2004JD005090.
- Zhang F. 2004. Generation of mesoscale gravity waves in upper-tropospheric jet-front systems. *J. Atmos. Sci.* **61**: 440–457.